Electrical Engineering

Golden section search based maximum power point tracking strategy for a dual output DC-DC converter

R. Gayathri *, G.A. Ezhilarasi

School of Electrical Engineering, VIT University, Chennai Campus, India

ARTICLE INFO

ABSTRACT

This paper introduces an Golden Section Search based algorithm, along with an single input multi output DC-DC converter for photovoltaic systems. In contemplation for photovoltaic (PV) systems to escalate their efficiency of power generation, it is mandatory to locate the Maximum power point (MPP) under all possible illumination conditions. Maximum power point tracking (MPPT) controller is expected to obtain the MPP irrespective of the device and climatic changes. The basic principle and the implementation of the system is elaborated in this paper, along with an comparison of different hill-climbing algorithms. The analytic and simulated results show that the new method has the advantages of fast convergence, noise-resistance, and robustness.

1. Introduction

In day to day life, there is an increase in the power density due to development of power electronics and material science. Renewable energy sources plays an crucial role to accommodate the power demand. Hence, it is essential to come up with inventive explications to cut down and preserve energy use. Solar energy is one of the most significant source of energy. In the last two decades, photovoltaics (PV), also known as solar PV, has emerged from a small scope applications towards becoming a dominant electricity provenience [1,4].

Maximum power point tracking (MPPT) is an approach that maximizes the output power to get better efficiency and many algorithms have been proposed to track the maximum power point using current as search parameter [2,3]. Under abruptly changing weather conditions (irradiance level) as MPP changes continuously, Perturb and Observe takes it as a change in MPP due to perturbation rather than that of irradiance and sometimes ends up in calculating wrong MPP [11]. However this problem gets avoided in Incremental Conductance method as the algorithm takes two samples of voltage and current to calculate MPP. However, instead of higher efficiency the complexity of the algorithm is very high compared to the previous one and hence the cost of implementation increases. So we have to mitigate with a trade off between complexity and efficiency and also these methods are derivative based and noise sensitive. A computational ease with inherent robust MPPT using golden section search (GSS) based algorithm is proposed in this paper. This is having noise and signal fluctuation immunity with fast convergence as compared to many reported MPPT methods [3,4]. This GSS based MPPT method is easy to implement on the low cost hardware with single current sensor and uses directly, the DC/DC converter duty cycle as a control parameter. In this paper, voltage is used as the search parameter.

It is also seen that the efficiency of the system depends upon the converter. Various single input multi output system is designed to satisfy the different voltage level requirements but these results in system complexity due to hard switching [7,8]. A simple duty cycle based pulse width modulation (PWM) is suggested. The switching and reverse recovery losses are less in the two-level boost converter. A hardware prototype of the converter is built and the control is made cost effective using ATMEGA based low cost controller. Both the simulation and hardware results are seen to have clear agreement with inherent robustness built using new MPPT algorithm.

This paper is organized as follow: Section 2, gives the system characterization. Section 3, gives the maximum power point algorithm techniques and Section 4 gives the simulated and Section 5, the hardware results and at last Section 6, concludes the paper, followed by the references.

* Corresponding author.
E-mail addresses: gayathri.r2014@vit.ac.in (R. Gayathri), angelineezhilarasi.g@vit.ac.in (G.A. Ezhilarasi)

Peer review under responsibility of Ain Shams University.

Production and hosting by Elsevier

Please cite this article in press as: Gayathri R, Ezhilarasi GA. Golden section search based maximum power point tracking strategy for a dual output DC-DC converter. Ain Shams Eng J (2017), http://dx.doi.org/10.1016/j.asej.2017.04.008

2. System description

The overall block diagram of the system is as shown below in the Fig. 1. This system consists of an PV module interfaced with the load through an DC-DC Converter. The pulse to the converter is given through the maximum power point tracker. The characteristics of each block are explicated in the following sections.

2.1. Modeling of solar cell

A solar cell is an electrical appliance, that converts the energy of light directly into electricity by the photovoltaic effect. In other words, a solar cell is defined as a device whose electrical characteristics, such as current, voltage, or resistance, vary when disclosed to light. Solar cells are the building blocks of photovoltaic modules, otherwise known as solar panels. It can be represented in two ways namely, single diode model and two diode model. In this paper, we consider the single diode model [4]. The proportionate circuit of an single diode model of a solar cell is as given below in the Fig. 2. Solar cells comprises of a p-n junction, fabricated in the layer of semiconductors, whose electrical characteristics diverges marginally from a diode, characterized by the equations given below. As shown in the figure, it comprises of an current source which is in parallel with the diode, wherein the output of the current source is directly reciprocal to the amount of light falling on the cell. The modeling of the cell is as shown below:

$$I = I_{pvcell} - I_{diode} \tag{1}$$

where

I_{pvcell} is the current due to the incidence of light,
I_{diode} is the Shockley diode equation,

The fundamental equation of the primary PV system given above does not produce the I-V characteristic of practical PV arrays. Practical modules consists of several connected PV cells that requires the inclusion of additional parameters such as Rs and Rp, which are as given below:

$$I = I_{pv} - I_o \left[exp \left(\frac{V + IR_s}{\alpha V_t} \right) - 1 \right] - \frac{V + IR_s}{R_p} \tag{2}$$

The current due to the light produced by the module calculates linearly on solar irradiation and temperature, which is given by the following equation:

$$I_{pv} = (I_{pv,n} + \Delta T K_I) \frac{G}{G_n} \tag{3}$$

where

K_I is the temperature coefficient of short circuit current,
G is the irradiance,
G_n is the irradiance at standard operating conditions,
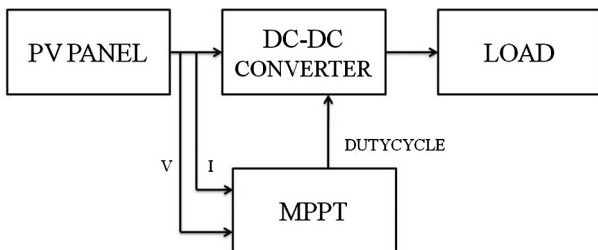q is the electron charge,

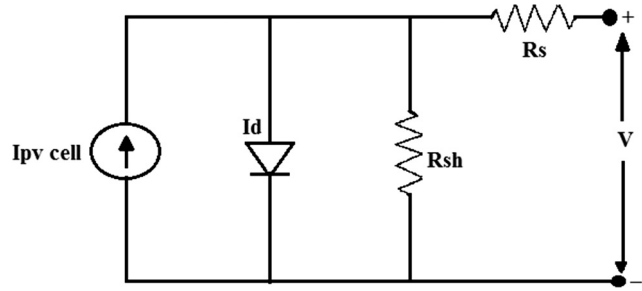**Fig. 1.** Overall block diagram of the system.

Fig. 2. Circuit diagram of pv cell.

k is the Boltzmann constant,
ΔT is the product of actual and nominal temperature of the p-n junction.

The diode saturation current Io depends on temperature and can be expressed by the following equation:

$$I_o = I_{o,n} \left(\frac{T_n}{T} \right)^3 \left[exp \left[\frac{q E_g}{k \alpha} \left(\frac{1}{T_n} - \frac{1}{T} \right) \right] \right] \tag{4}$$

where

E_g is band gap energy of semiconductor
$I_{o,n}$ is nominal saturation current

The final output current equation of a solar cell is as given below:

$$I_o = \frac{I_{sc,n} + K_I \Delta T}{e \left[V_{oc,n} + \left(\frac{K_v \Delta T}{V_t \alpha} - 1 \right) \right]} \tag{5}$$

where

$V_{oc,n}$ is open circuit voltage,
$I_{sc,n}$ is short circuit current,
V_t is thermal voltage,
T is the temperature at standard operating conditions.

2.2. DC-DC converter modeling

In this paper, a single input multi output converter is designed for the output voltage range of 15 V as an auxiliary voltage and 65 V as a high voltage with the input range of 35 V [3]. The circuit is simulated using MATLAB software and the high output voltage is regulated with the help of PI controller as a feedback path. This converter is helpful in those photovoltaic applications where dual output is required from a single input. The circuit diagram of the converter is as shown in the Fig. 3. The converter consists of five sections namely low voltage circuit, middle voltage circuit, clamped circuit, auxiliary circuit and high voltage circuit. From the circuit it is seen that, C_{01} and C_{02} are the filter capacitors that are used in the corresponding low and high side output voltages. C_1 and C_2 are the capacitors, which are used for the clamped and middle circuit. L_p and L_s are the primary and secondary side of a coupled inductor. L_{aux} is the auxiliary inductor. This converter consists of six modes of operation.

MODE:1 In this mode, the switch S is turned ON. The dc supply flows through the primary of the inductor, and the diode $D2$ will be in conducting mode. Due to the positive polarity across the circuit, which is as shown in the Fig. 4, the secondary of the coupled inductor will have a reverse current, which will charge the capacitor C_2 with the help of diode $D3$ and the diode $D4$ will
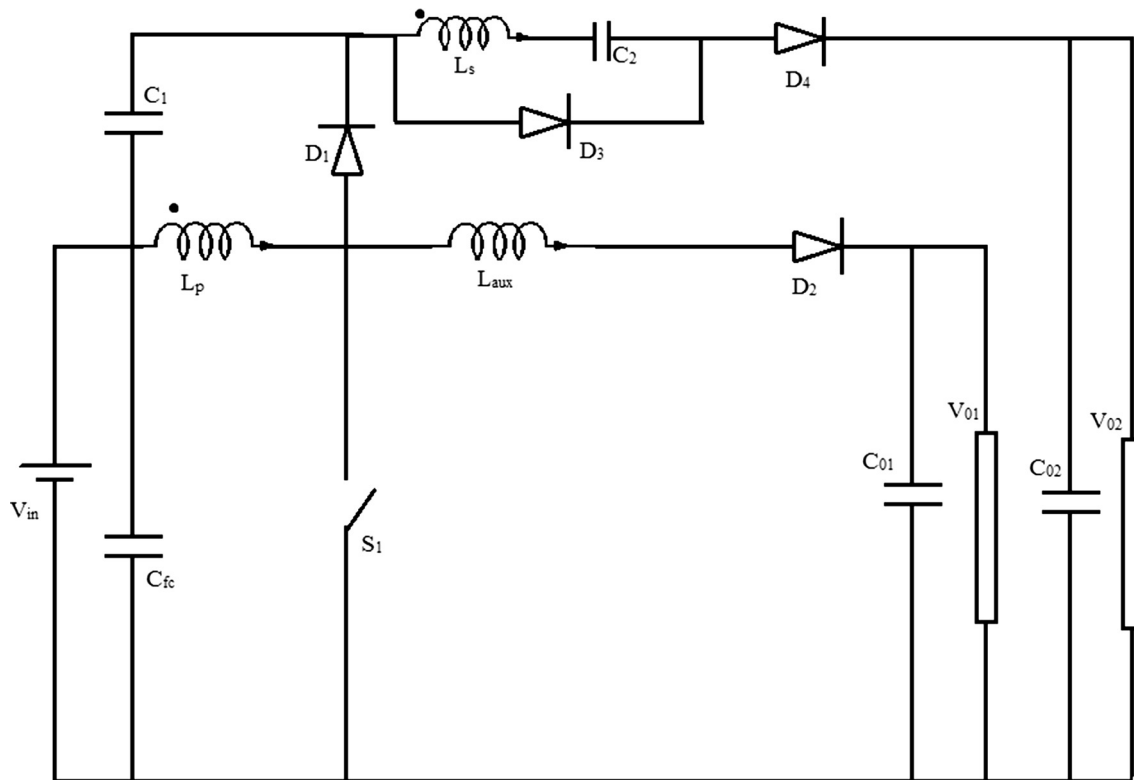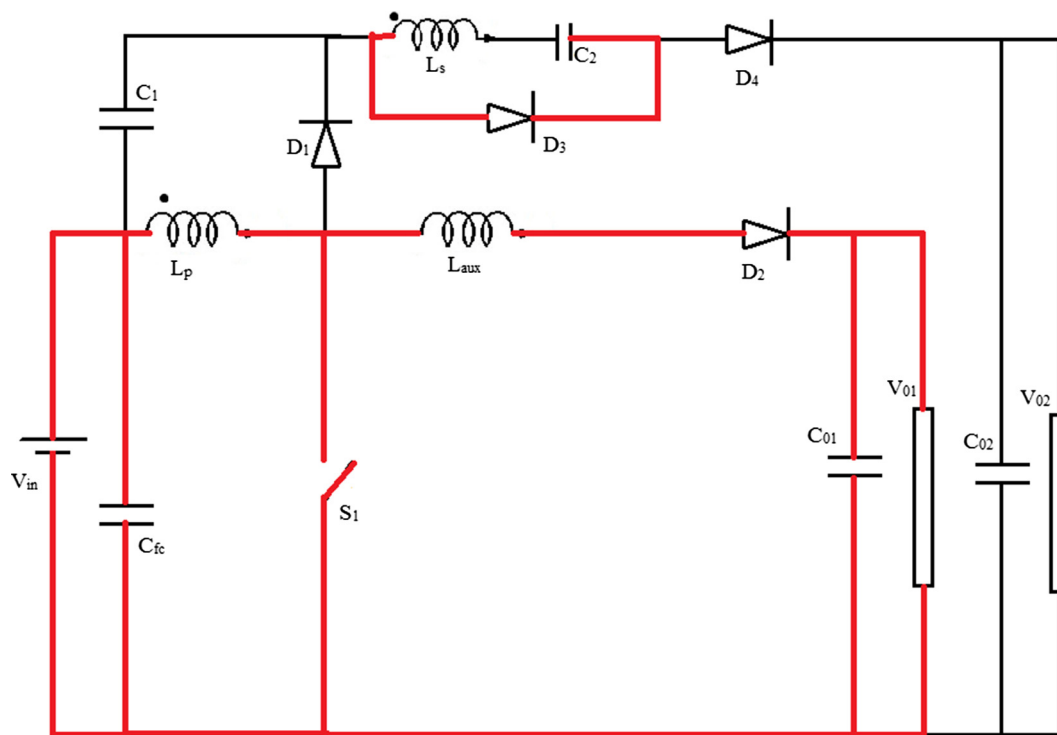
Fig. 3. Circuit diagram of the converter.

Fig. 4. Current path in mode 1.

remain in non conducting mode. This mode ends, when the energy in L_{aux} will be completely discharged.

MODE:2 In this mode, the switch will be in ON condition but the diode $D2$ will be in OFF condition, whereas the capacitor C_2 will be charging, by the reverse current of the secondary inductor and the primary of the coupled inductor will receive supply from the dc source. Though the switch is in ON condition, for both mode 1 and mode 2, the current of the coupled

inductor will be different, due to the auxiliary inductor present in the circuit (see Fig. 5).

MODE:3 In this mode, the switch is turned OFF. The voltage across the switch will be higher than that of the clamped capacitor, thereby making the diode $D1$ to conduct. The energy from the primary of the coupled inductor will be distributed to the auxiliary inductor and the capacitor. As the auxiliary inductor tends to charge, the diode $D2$ will conduct which will supply the corresponding output power to the load in auxiliary circuit as shown in Fig. 6.

MODE:4 As the switch is in OFF condition as seen in Fig. 7, once the reverse current completely charges the clamped capacitor, the diode $D3$ will not conduct. Hence the secondary inductor, clamped capacitor and the diode $D4$ will be connected in series, which generates power to the output of the high voltage side.

MODE:5 In this mode, the switch is in OFF condition, once the voltage of primary inductor and auxiliary voltage are equal, the diode $D1$ will be in OFF state. At this time, the primary inductor and the auxilliary inductor will be connected in series, which makes the diode $D2$ to conduct and generates the output power on auxiliary load voltage, The current path in this mode is shown in the Fig. 8.

MODE:6 When the switch is triggered, the diode $D3$ and $D1$ will be in OFF state as shown in Fig. 9. The auxiliary inductor will be charged with the help of primary inductor which makes the diode $D2$ to conduct and will generate the required output power. Meanwhile the secondary inductor and the clamped capacitor will be connected in series which makes the diode $D4$ to conduct and generate its corresponding high output power. This mode ends when the secondary power comes to zero.

Due to the presence of auxiliary inductor, the proposed SIMO converter operates in continuous conduction mode (CCM). When the switch is in ON condition the couple inductor gets charged and discharges its energy when the switch is in OFF condition.

2.2.1. Design considerations

The turn's ratio (N) and coupling coefficient of the transformer is given by

$$N = \frac{N_2}{N_1} \tag{6}$$

$$k = \frac{L_s}{L_p} \tag{7}$$

where N_1 and N_2 are the turns ratio of the coupled inductor and k is the coupling coefficient. By using volt-sec balance on the primary of the inductor,

$$V_{in}T_{on} + V_{lp}T_{off} = 0 \tag{8}$$

where

$$V_{lp} = -\frac{d_1}{(1-d_1)V_{in}} \tag{9}$$

$C_1 = -l_p$ during the modes 3 and 4 $V_{c1} = -V_{lp}$ Thus, by applying KVL to the outer circuit, we get the following equations,

$$V_{LS}T_{on} + V_{LS}T_{off} = 0 \tag{10}$$

$$G_{VH} = \frac{V_{02}}{V_{in}} = \frac{(N+1)}{1-d_1} \tag{11}$$

During the modes 1 and 6,

$$d_x T_s = [(t_6 - t_5) + (t_1 - t_0)] \tag{12}$$

Now by applying volt sec on auxiliary inductor, we get the following equations,

$$T_{on} + V_{Laux}T_{off} = 0 \tag{13}$$

$$-V_{01}(d_x T_s) + (V_{in} - V_{LP} - V_{02}) \times (1-d_1)T_s = 0 \tag{14}$$

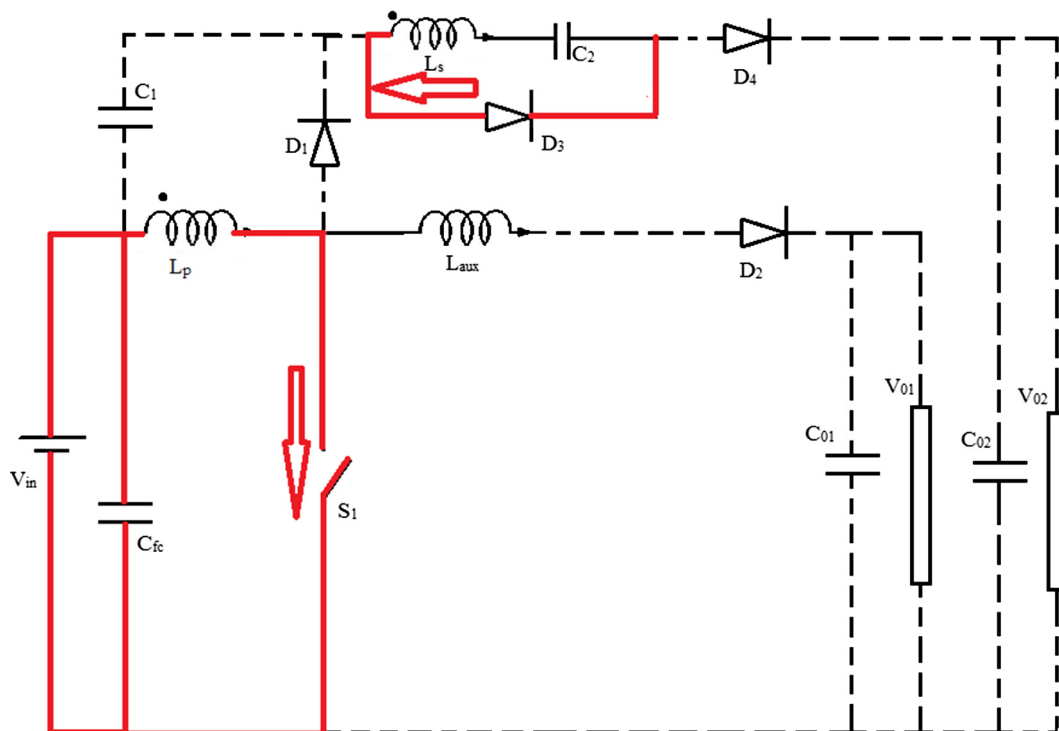The electric charge variation for the auxiliary output is given by

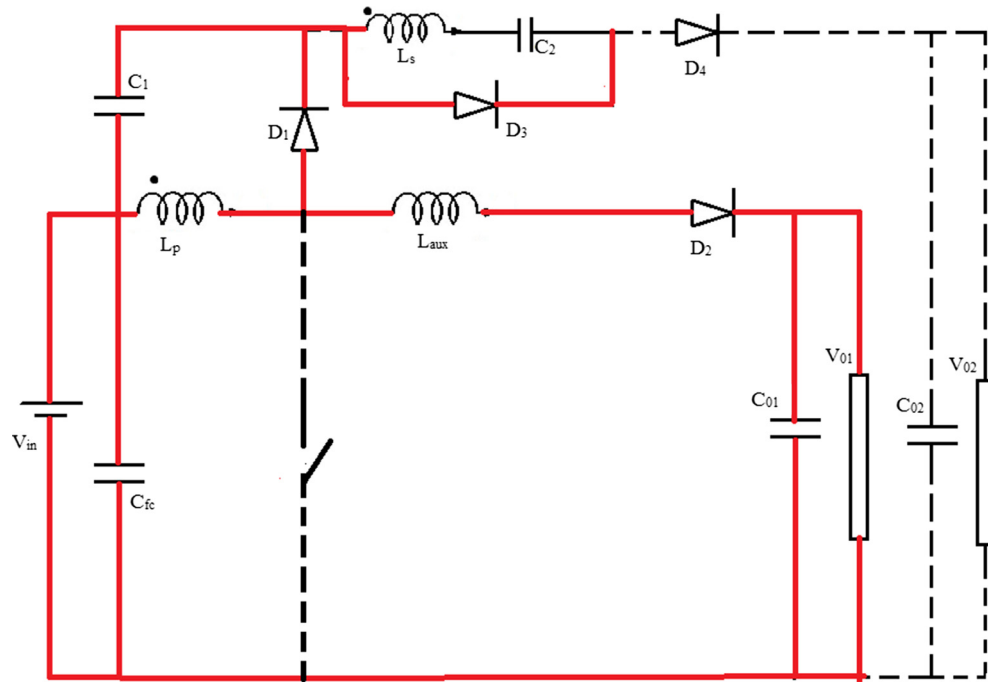**Fig. 5.** Current path in mode 2.
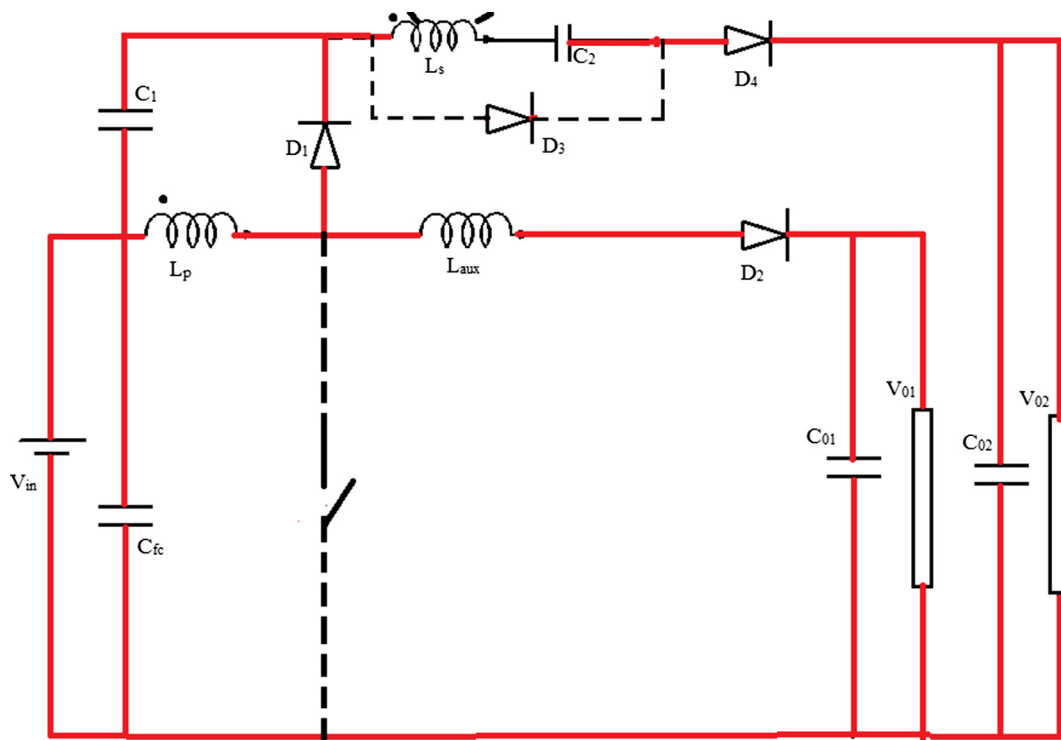
Fig. 6. Current path in mode 3.

Fig. 7. Current path in mode 4.

$$\delta Q_1 = \frac{V_{01}}{R_{01}} \times (d_1 - d_x) \times T_s = C_{01}\delta V_{01} \qquad (15)$$

The electric charge variation for the high side output is given by

$$\delta Q_2 = \frac{V_{02}}{R_{02}} \times (d_1) \times T_s = C_{02}\delta V_{02} \qquad (16)$$

where δV_{01} and δV_{02} is the ripple factor which should be less than 1.

Fig. 8. Current path in mode 5.

Fig. 9. Current path in mode 6.

$$C_1 = \frac{1}{(f_{01})^2 4(^2) L_P} \qquad (17)$$

$$C_2 = \frac{1}{(f_{02})^2 4(^2) L_s} \qquad (18)$$

The cut off frequencies of L_p and L_s should be 10 times lesser than the switching frequencies.

3. Maximum power point tracking algorithms

Maximum power point tracking (MPPT) is an approach used by charge controllers for wind turbines and PV solar systems to maximize power output. PV solar systems occurs in several configurations. Solar cells have a convoluted link between temperature and total resistance that gives a non-linear output efficiency which can be evaluated based on the I-V curve [2]. It is the objective of the

MPPT system to fragment the output of the PV cells and employ proper resistance (load) in order to obtain the maximum power for any given environmental conditions. MPPT devices are commonly integrated into an electric power converter system that provides voltage or current conversion, filtering and regulation for driving various loads, including power grids, batteries, or motors [3].

According to Maximum Power Transfer theorem, the power output of a circuit is maximum when the Thevenin impedance of the circuit (source impedance) matches with the load impedance. Hence, the problem of tracking the maximum power point reduces to an impedance matching problem. In the source side, we are using a SIMO converter connected to a solar panel in order to enhance the output voltage, so that it can be used for different applications like Solar powered vehicles. By changing the duty cycle of the converter appropriately, we can match the source impedance with that of the load impedance.

3.1. Existing hill climbing methods

Perturb and Observe (P&O) is the simplest hill climbing method. In this we use only one sensor, that is the voltage sensor, to sense the PV array voltage and so the cost of implementation is less and thereby, easy to implement. The time complexity of this algorithm is very less. In several studies, it has been shown that P&O has led to efficiencies as high as 96.5 in [8], and 99.5 in [9]. Incremental conductance method uses two voltage and current sensors to sense the output voltage and current of the PV array. The controller, measures the incremental changes in PV array current and voltage, in order to predict the effect of change in the voltage. A PI controller

is an effective way of implementing the InCond algorithm. The efficiency of this algorithm is higher than P&O, [8] states an efficiency of 98.5 in simulation and 98.2 in measurements.

3.2. Drawbacks of hill climbing methods

The two algorithms mentioned above have certain, similar drawbacks. First, all of them can not distinguish a local maximum from a global maximum. In case of shaded conditions, these local maxima do occur in the *p-v* characteristic of a solar panel and operating at a local maximum could mean reduced power output. Secondly, all algorithms mentioned have irregular behavior in case of rapidly changing irradiation conditions [3,9,10]. In both these cases, it is possible the algorithm loses track of the MPP and reduced power output will occur [12–15].

3.3. Golden section search method

The golden section search is a technique that is used for discovering the minimum or maximum of a strictly uni-modal function by individually narrowing the range of values inside which the extremum is known to exist [5]. This method is vigorous and also has a faster feedback compared to the other traditional algorithms. The main aim is to find maximum functional value within the input interval [*a,b*]. Two points are selected in the interval [*a,b*] and the function is evaluated at these points. Points are selected in such a way that each point subdivides the interval into two parts and length of whole line/length of larger fraction = length of larger fraction/length of smaller fraction. Assume a line segment as shown in Fig. 11. It gives from 0 to $v_o c$. The
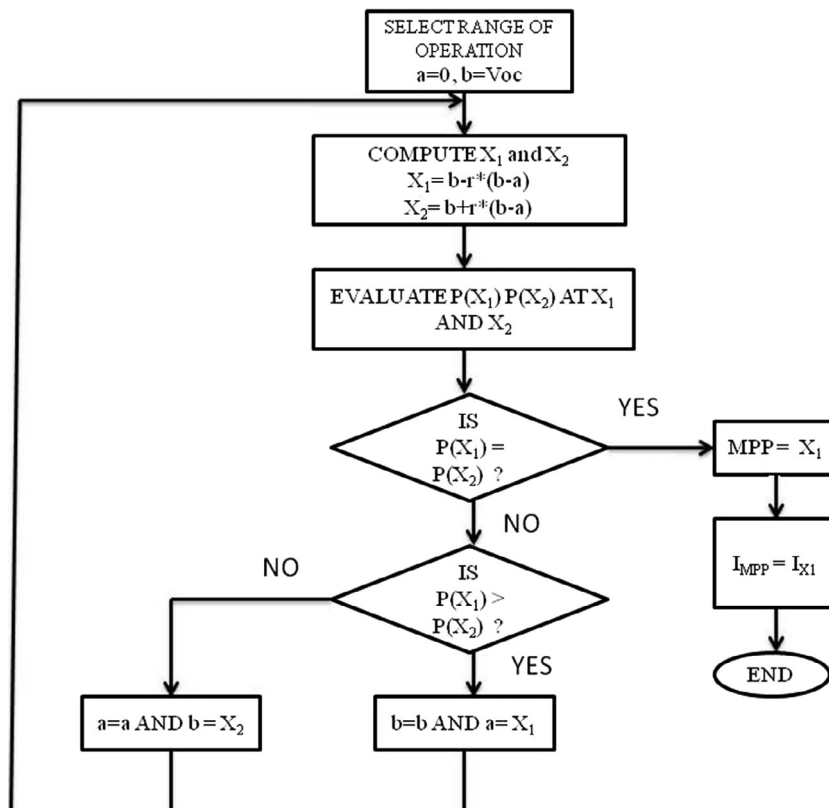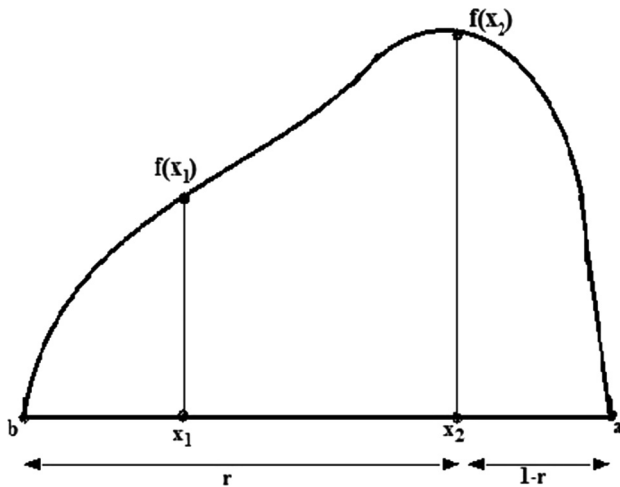
Fig. 10. Flowchart of the algorithm.

Fig. 11a. Division of intervals.

Table 2
Parameters of panel at standard conditions.

S. no	Parameters	Value
1	Peak power	250 W
2	Maximum voltage	35.80 V
3	Maximum current	8.30 A
4	Output voltage	200 V
5	Output current	1.2 A

Table 3
Simulated values.

S. no	Parameters	Simulated value
1	Input voltage	35 V
2	Input current	8.27 A
3	Input power	248 W
4	Reverse saturation current	$2.623 \times (10e{-}7)$
5	Saturation current	$5\ 2.623 \times (10e{-}7)$
6	Short circuit current	6 8.2 A
7	Maximum power point	200 W

length from b to X_1 is given by r and the length from X_2 is given by $1 - r$. The values are calculated using the formulas given in the flowchart above, and the corresponding powers are calculated at these points and the rest of operation is as illustrated in the flowchart. For a GSS based MPPT for photovoltaic system, the PV characteristics are the operating characteristics wherein the main function corresponds to power, whose maximum value has to be captured. The spectrum of operation is from zero to open circuit voltage (Voc); that is, $a = 0$, $b = $ Voc with $r = 0.618$ [6]. The way of tracking maximum point is shown in the Fig. 10. The voltage corresponding to the maximum power is obtained and mapped into the V-I characteristics to achieve the current reference.

3.4. GSS with voltage as search parameter

The detailed GSS algorithm at standard operating conditions that is, G = 1000 W/m^2 and temperature at 25 °C and with an open circuit voltage of 30 V is as given below in the Table 1.

4. Simulation results

4.1. PV module simulation

The PV Module Simulation is done in MATLAB. The simulation is done at standard conditions in order to check the MATLAB model
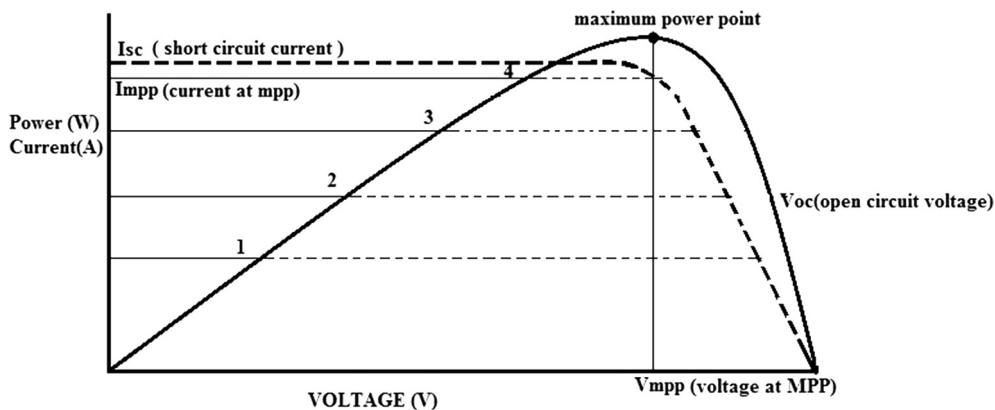

Fig. 11b. MPPT tracking.

Table 1
Search algorithm at standard operating conditions.

Step	a	b	x_1	x_2	P_1	P_2	Comment
1	0	30	13	20	98	155	$P_2 > P_1$
2	13	29.9	21	25	163	192	$P_2 > P_1$
3	21	32.9	25	28	192	199	$P_2 > P_1$
4	25	32.9	28	30	199	176	$P_1 > P_2$
5	25	28	26	27	197	200	$P_1 > P_2$
6	25	28	26	27	197	200	$P_2 > P_1$
7	26	28	27	27	200	200	$P_1 = P_2$

PV Panel. The Input to the panel is given according to the datasheet of the panel used which is given in the table. The unknown parameters are evaluated and power-voltage and current–voltage characteristics are simulated. The unknown parameters, saturation current at reference temperature Ior, saturation current Io and Short circuit current Isc at the given temperature are calculated from the input parameters which is given in the Table 3.

In this paper, ELDORA VSP.60.AAA.03 silver series/Polycrystaline solar PV modules are used. The Table 2 shows its electrical specifications from the datasheet. In this PV module, 60 cells are connected in series–parallel combination. All the technical data's are taken at standard test condition, that is, at an standard irradiance level of 1000 W/m^2 and at an temperature $T = 25\,°C$. The Table 3 gives the simulated output and input parameters to the panel. The unknown parameters are saturation current at reference temperature Ior, saturation current Io and Short circuit current Isc at the given temperature are calculated from the input parameters.

4.1.1. Variation of IV and PV curve at different irradiation

In order to verify the model under different operating conditions, several tests have been performed at various temperature and solar irradiance values. The Figs. 12a and 12b shows the IV curves and PV curves for various solar irradiance G varies from 600 W/m^2 to 1000 W/m^2 at standard cell temperature of 25 °C.

From the curves it is seen that, PV curve has negligible effect on the open circuit voltage, due to the variation of irradiation and mainly affects short circuit current.

4.1.2. Variation of IV and PV curve at different temperature

The IV characteristics with constant radiation and different temperature are shown in Fig. 13. It is seen from the curve that IV curve has negligible effect on the short circuit current due to the variation of temperature and mainly affects open circuit voltage.
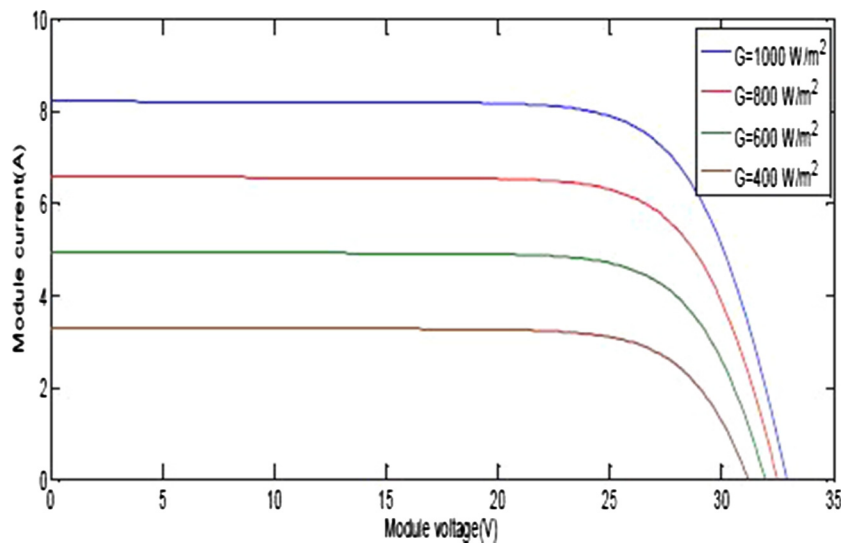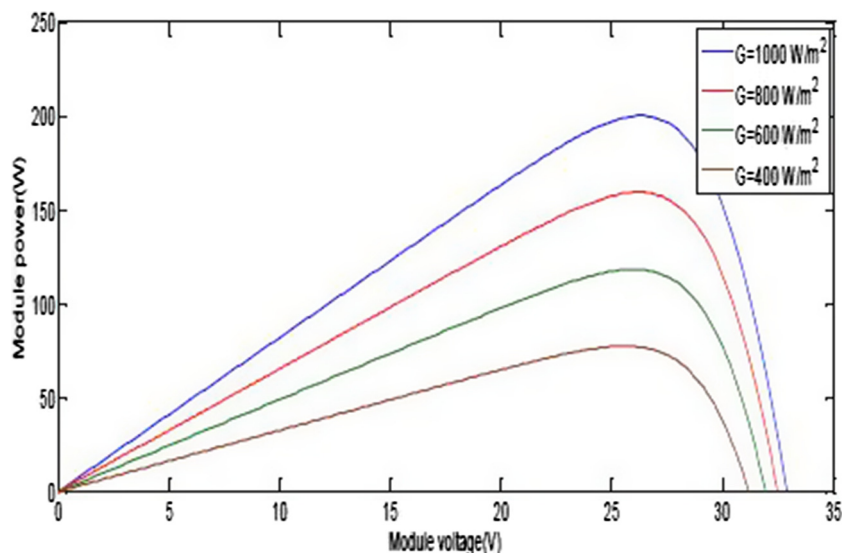

Fig. 12a. Variation of IV curve
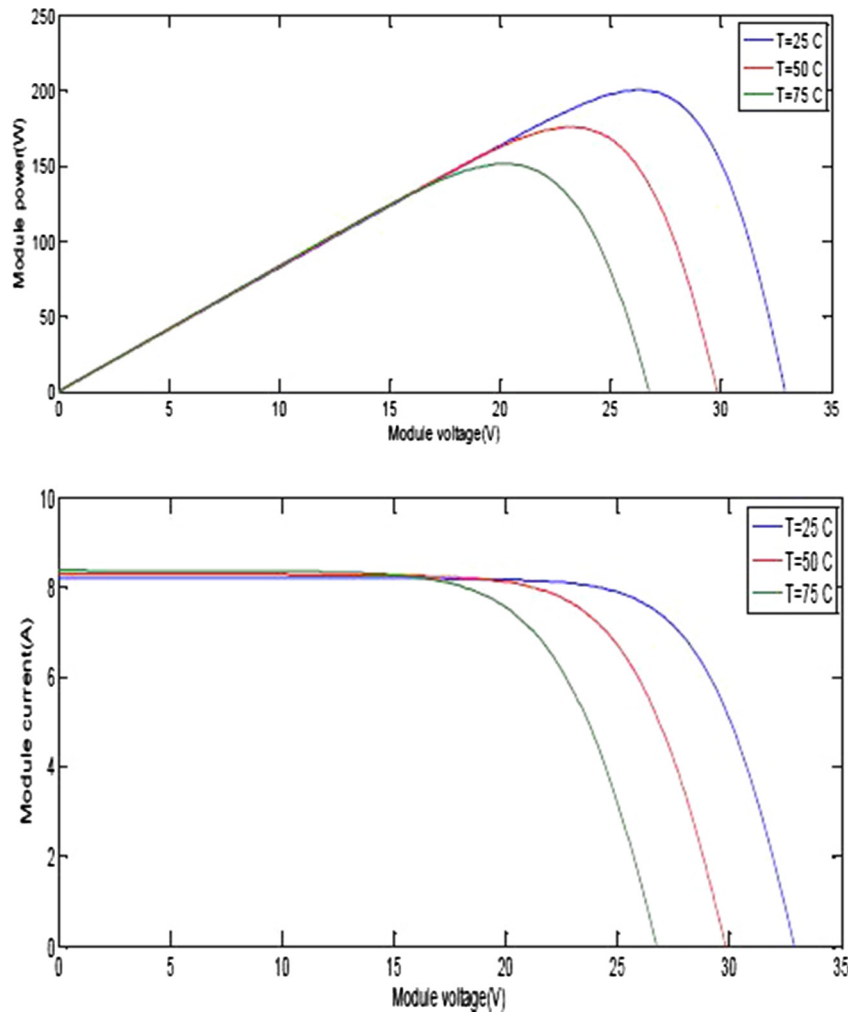

Fig. 12b. Variation of PV curve.

Fig. 13. Variation of curves at different iradiation.

Table 4
Duty cycle for different irradiations.

S. no	G	V_{in}	I_{in}	P_{in}	D	V_{out}	I_{out}	P_{out}
1	600	25	8.20	205	0.25	48	4.21	205
2	800	28	8.23	229	0.37	52	4.42	229.8
3	1000	30	8.29	247	0.5	59	4.25	247.8

4.2. Maximum power point tracking simulation

The algorithms were tested at various irradiation conditions and the value was recorded. The Table 4 shows the variation of duty cycle for different irradiation conditions.

The duty cycle obtained from the maximum power point block in order to drive the switch is as shown in the Fig. 14. It gives the variation of duty cycle at various operating conditions.

The system is tested for both open loop i.e. without MPPT and closed loop i.e. with MPPT, Readings for both the conditions was taken with intervals of time for whole day. Readings were tabulated and the impedance curve was plotted which is as shown in Fig. 15. From the Graph Fig. 15b it is seen that, impedance of load and source will be different as there is no MPPT, hence only partial transfer of power occurs, whereas, Graph Fig. 15a gives the impedance curve while using MPPT. From the graph it is interpreted that the MPPT algorithm matches the load impedance with the

source impedance, which is the condition for maximum power transfer.

4.3. Converter simulation

The proposed converter was simulated using the MATLAB software tool. This results were verified with that of hardware results. The Fig. 16a shows the open loop simulation results of the proposed system. For the input voltage of 35 V the output voltages of 15 V and 65 V is obtained. Where 15 V is considered to be the auxiliary voltage and can be used for charging the batteries. The voltage 65 V is considered as a high output voltage and used in high level inverters. From the Fig. 16b it is inferred that, the output currents are less when compared to that of the input current which proves that the system acts as a boost converter.

Fig. 16c shows the zero current switching of the converter. When the voltage is zero and corresponding current increases then
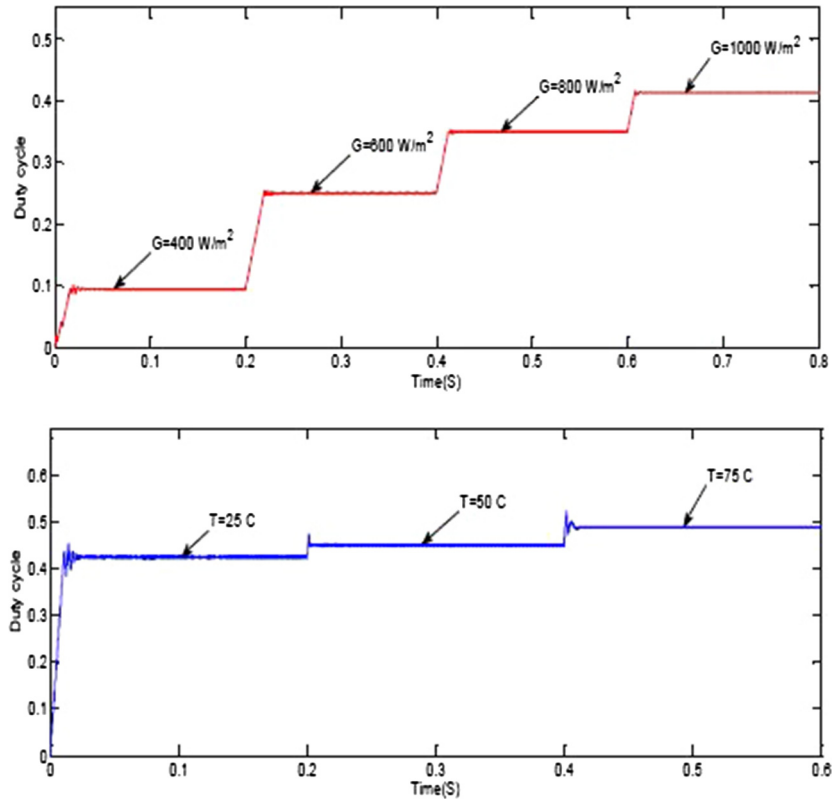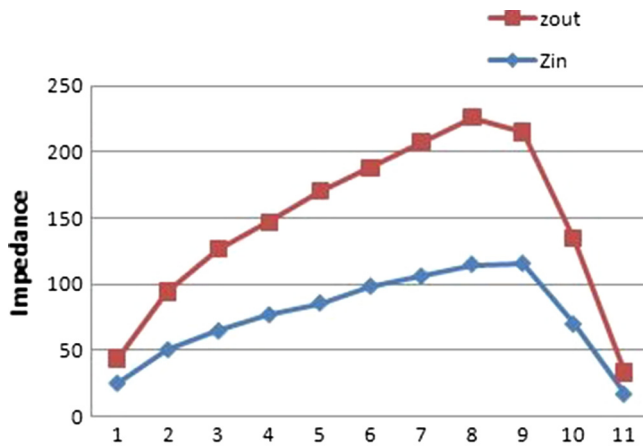
Fig. 14. Duty cycle at different conditions.
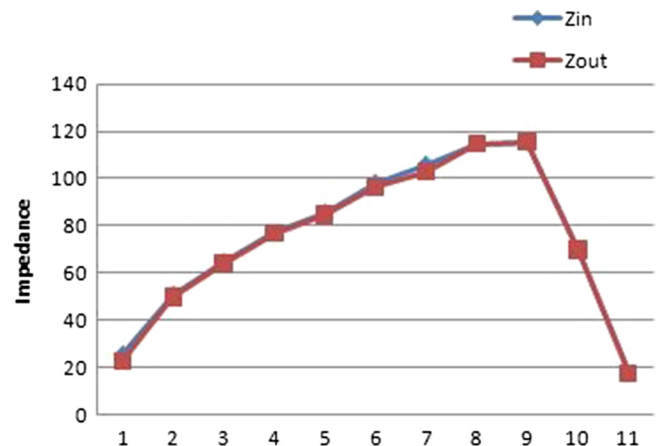

Fig. 15a. Impedance curve without mppt.

Fig. 15b. Impedance curve with mppt.

the condition is known as zero current switching and hence, due to this, the switching losses will be reduced.

5. Hardware results

The hardware setup of PV standalone system with PV module is tested at 240 W power with a frequency of 72 KHz. The DC-DC converter, Arduino Uno board ATMEGA328, MOSFET driver circuit and power supply unit are integrated. Voltage and current sensors are used in order to sense the respective voltage and current from the panel. The Table 5 below gives the designed electrical specifications of the converter.

The whole setup was analyzed and the maximum power point algorithms were implemented using ATMEGA328. The duty cycle

obtained is as shown in Fig. 17a at standard operating conditions. The zero current switching of this converter in hardware is shown in Fig. 17b. When comparing both the simulation and hardware results, it is clear that ZCS is obtained.

Fig. 18a shows the charging and discharging of the inductor when the switch is in ON and OFF condition. In the figure, channel 1 shows the gate pulses and channel 2 inductor current. Fig. 18b shows the output voltage at standard operating conditions, with an input voltage of 35 V, an output voltage of 65 V is obtained, which can be further used for grid interface or for inverters and also an output of voltage of 15 V, which can be further used for battery charging and the ouput voltage is as obtained in the Fig. 19.

The output parameters are as obtained above. The gain of the converter is as obtained below, when the duty cycle from the
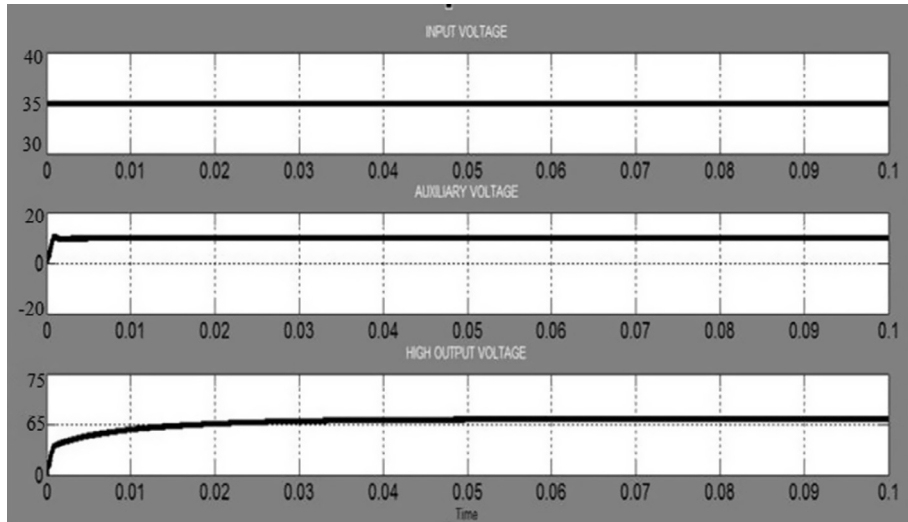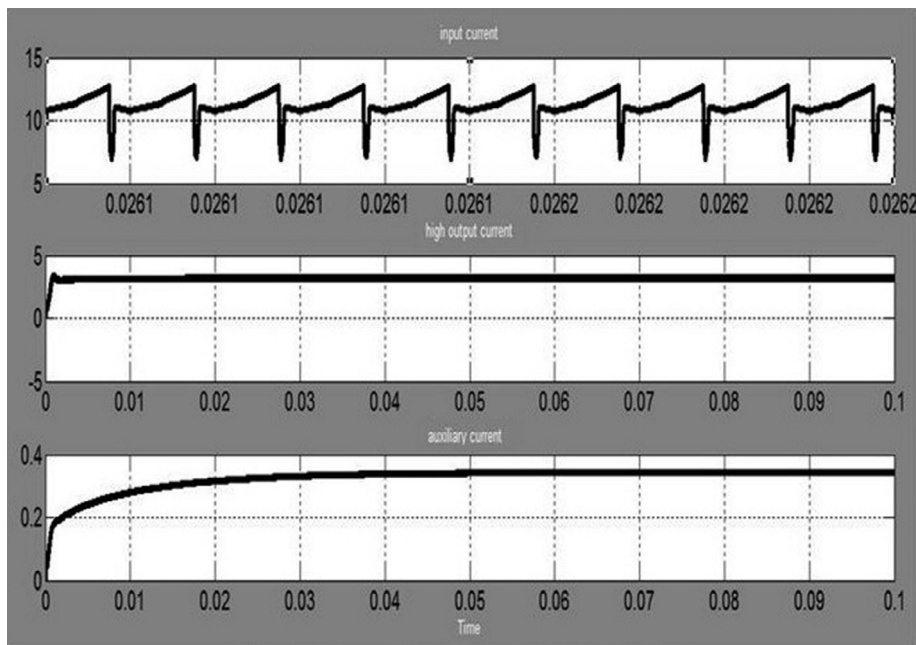
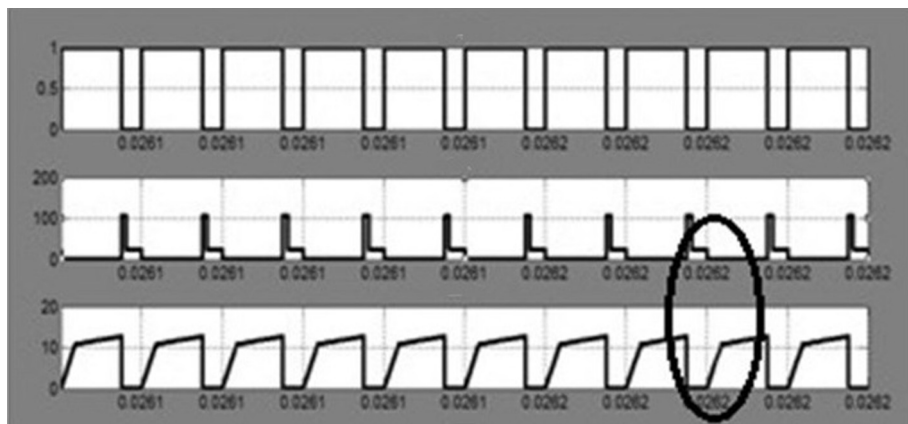**Fig. 16a.** Output parameters.

Fig. 16b. Current waveforms.

Fig. 16c. ZCS condition.

Table 5
Designed electrical specifications.

Parameters	Designed values
L_{aux}	2.2 μH
L_p	55 μH
L_s	75 μH
C_1	80 μF
C_2	10 μF
C_{01}	75 μF
C_{02}	100 μF

Fig. 18a. Buck voltage.

Fig. 17a. Duty cycle.

Fig. 18b. Boost voltage.

Fig. 17b. ZCS condition.

Fig. 19. Current across inductor.

maximum power point tracker varies. They are plotted as shown below in the Fig. 20. From the graph it is seen that, when the duty cycle to the converter increases, the gain also increases which implies that they are in proportion.
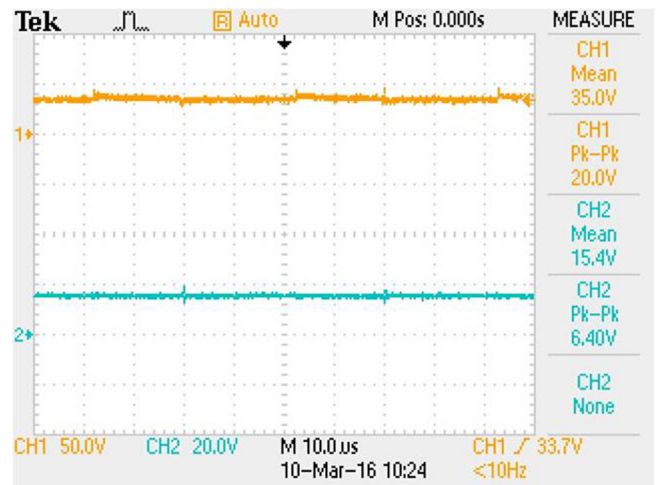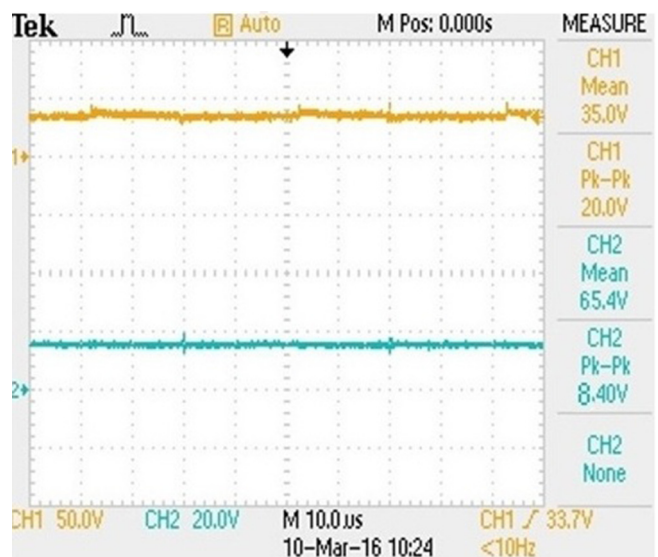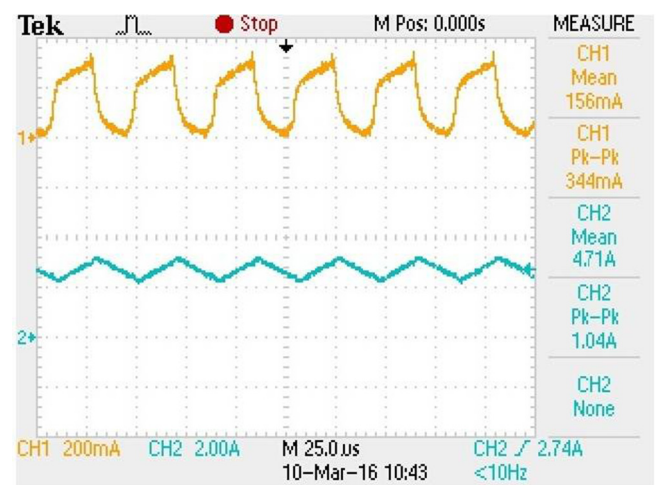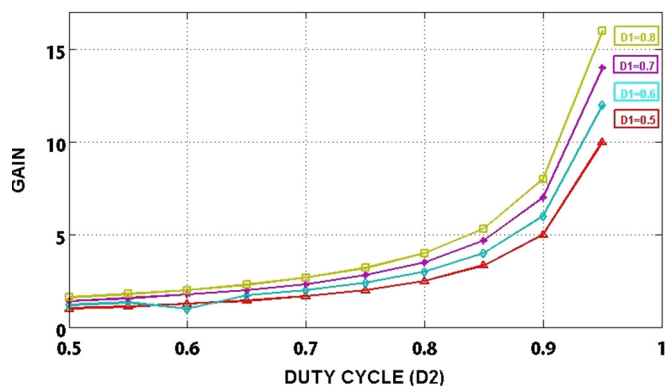
Fig. 20. Voltage gains of the converter.

6. Conclusions

In this work, it is inferred that the current–voltage relationship is non linear and there is a maximum power at a peculiar current and voltage. This maximum power is varying with regard to the atmospheric conditions. In this paper, evaluation with regard to the changes in the effect of irradiation and atmospheric temperature on current - voltage characteristics and power - voltage characteristics are studied. When the irradiation level decreases, the photo generated current goes down significantly. The open circuit voltage (Voc) also drops, but the effect is negligible. In decreasing atmospheric temperature value, at solar irradiation of 1000 W/m^2, open circuit voltage is only decreased and the photo generated current remain constant. The performance of the MPPT with GSS based algorithm indicates good agreement with the simulated results. This indicates the converter performance with its efficiency up to 90 is achieved.

References

[1] Ramos Hernanz JA, Campayo Martin JJ, Zamora Belver I, Larranga Lesaka J, Zulueta Guerrero E. Modeling of photovoltaic module. In: International conference on renewable energies and power quality (ICREPQ'10) Granada (Spain), 23th to 25th March; 2010.

[2] Esram T, Chapman PL. Comparison of photovoltaic array maximum power point tracking techniques. IEEE Trans Energy Convers 2007;22(2).

[3] Balato Marco, Costanzo Luigi, Vitelli Massimo. Maximum power point tracking techniques. Wiley Encyclopedia of electrical and electronics engineering. Published Online: 15 FEB 2016.

[4] Balato Marco, Costanzo Luigi, Vitelli Massimo. Reconfiguration of PV modules: a tool to get the best compromise between maximization of the extracted power and minimization of localized heating phenomena. Sol Energy 2016;138(November).

[5] Chen H-C, Lin W-J. MPPT and voltage balancing control with sensing only inductor current for photovoltaic-fed, three-level, boost-type converters. IEEE Trans Power 2014;29(1):29–35.

[6] Ghaffari A, Seshagiri S, Krsti'c M. High-fidelity PV array modeling for advanced MPPT design. In: Proc. of IEEE Canadian conference on electrical and computer engineering (CCECE); 2012.

[7] De Brito MAG, Galotto L, Sampaiode LP, Azevedo e Melo G, Canesin CA. Evaluation of the main MPPT techniques for photovoltaic applications. IEEE Trans Indust Electron 2013;60(2):1156–67.

[8] Lei T, Xu W, Chengbi Z, Jinhu L, Jinwei H. One novel variable step-size MPPT algorithm for photovoltaic power generation. In: 38th annual conference on IEEE industrial electronics society; 2012. p. 5750–5.

[9] Ahmed EM, Shoyama M. Single variable based variable step size maximum power point tracker for stand-alone battery storage PV systems. In: IEEE International Conference on Industrial Technology (ICIT); 2011. p. 210-6.

[10] Jordan DC, Kurtz SR. Photovoltaic degradation rates-an analytical review. Prog Photovolt Res Appl 2013;21(1):12–29.

[11] Kjaer SB. Evaluation of the hill climbing and the incremental conductance maximum power point trackers for photovoltaic power systems. IEEE Trans Energy Convers 2012;27(4):1292–306.

[12] Gaga Ahmed, Errahimi Fatima, Es-Sbai Najia. Design and implementation of MPPT solar system based on the enhanced P&O algorithm using labview. In: 2014 International Renewable and Sustainable Energy Conference (IRSEC), published in IEEE on 16 March 2015.

[13] Agrawal J, Aware M. Golden section search (GSS) algorithm for maximum power point tracking in photovoltaic system. In: Proceedings of the IEEE 5th India internationalconference on power electronics (IICPE '12), Delhi, India, vol. 6; December 2012. p. 1.

[14] Wai Rong-Jong, Jhang Kun Huki. High efficiency single input multiple output Dc-Dc converter. IEEE Trans Power Electron 2013;28(12).

[15] Kirubakaran A, Jain S, Nema RK. DSP-controlled power electronic interface for fuel-cell-based distributed generation. IEEE Trans Power Electron 2011;26(12):3853–64.